# Scaling of fracture and Acoustic Emission in the compression of concrete-like materials

Stefano Invernizzi[1], Giuseppe Lacidogna[1], Alberto Carpinteri[1]

[1]*Dipartimento di Ingegneria Strutturale e Geotecnica, Politecnico di Torino, Italy*
*E-mail*: alberto.carpinteri@polito.it; stefano.invernizzi@polito.it;
giuseppe.lacidogna@polito.it

*Keywords:* Acoustic Emissions; finite element method, size-effects.

SUMMARY. A combined compression and AE test is proposed, in order to study the scaling of fracture and Acoustic Emission in concrete-like specimens with different size and slenderness. The cylindrical concrete specimens were drilled from two pilasters sustaining a viaduct along an Italian highway built in the 1950s. A two-dimensional FEM numerical model of the pure compression tests is also presented, which is able to describe both the discrete cracking at the matrix-aggregate interface and the smeared cracking of the matrix. The adopted mesoscale modeling directly accounts for the aggregate dimensional distribution, being each aggregate explicitly represented. The distribution of aggregate size and position was generated according to the Füller distribution. In this way, the crack patterns can be simulated correctly, as well as the load displacement curve. During microcrack propagation, acoustic emission events can be clearly detected experimentally. Therefore, the number of acoustic emissions can be put into relation with the number of Gauss points in the finite element model where cracking takes place. A good correlation is found between the amount of cracking simulated numerically and the experimental acoustic emission counting for different specimen sizes, and the two quantities show the same exponent with respect to the considered volume. This evidence reconfirms the assumption, provided by fragmentation theories, that the energy dissipation during microcrack propagation occurs in a fractal domain comprised between a surface and the specimen volume.

## 1 INTRODUCTION

Nondestructive and instrumental investigation methods are currently employed to measure and check the evolution of adverse structural phenomena, such as damage and cracking, and to predict their subsequent developments. The choice of a technique for controlling and monitoring reinforced concrete or masonry structures is strictly correlated with the kind of structure to be analyzed and the data to be extracted [1,2].

This study addresses the pure compression test carried out in laboratory performed on drilled concrete cores obtained from two pilasters sustaining a viaduct along an Italian highway [3]. At the same time, the cracking processes taking place during the test was monitored using the acoustic emission (AE) technique. A similar approach has been already exploited in [4] attempting to link the amount of AE with the structural deflections.

In the assessment of structural integrity, the AE technique has proved particularly effective [4-6], in that it makes it possible to estimate the amount of energy released during the fracture process and to obtain information on the criticality of the process underway. Strictly connected to the energy detected by AE is the energy dissipated by the monitored structure. The energy dissipated during crack formation in structures made of quasi-brittle materials plays a fundamental

role in the behavior throughout their life. Recently, according to fractal concepts, an ad hoc theory has been employed to monitor structures by means of the AE technique [3-6]. The fractal theory takes into account the multiscale character of energy dissipation and the strong size effects associated with it. With this energetic approach, it becomes possible to introduce a useful damage parameter for structural assessment based on a correlation between AE activity in the structure and the corresponding activity recorded on specimens of different sizes, tested to failure by means of double flat-jacks or pure compression tests. The main achievement of the present work consists in showing how the amount of cracking obtained from the numerical simulation and the AE events share the same scaling laws.

## 2 COMBINED COMPRESSION AND AE TESTS

By means of the AE technique, we also analyzed the damage evolution in two pilasters sustaining a viaduct along an Italian highway built in the 1950s. From the pilasters we drilled some concrete cylindrical specimens in order to detect the mechanical properties of the material under compression and to evaluate the scale effects in size and time on AE activity [3].

Figure 1: Apparatus adopted for compression tests.

### 2.1 *Test specimens and testing equipment*

The cementitious material, of rather good mechanical characteristics, presents an apparent specific weight of about 2.22 g/cm$^3$ and a maximum aggregate size of about 15 mm. For each pilaster, three different specimen diameters d are considered in a maximum scale range of 1:3.4.

The specimens present three different slendernesses: λ = h/d = 0.5, 1.0 and 2.0, with d chosen equal to 27.7, 59, 94 mm, respectively. For each of these nine geometries, three specimens have been tested, for a total of 54 cases (two pilasters). The average values obtained from the experimental data are reported in Table 3. The system adopted in the compression test utilizes rigid steel platens, the lateral deformation of concrete being therefore confined at the specimen ends, which are forced to have the same lateral deformation as the rigid platens.

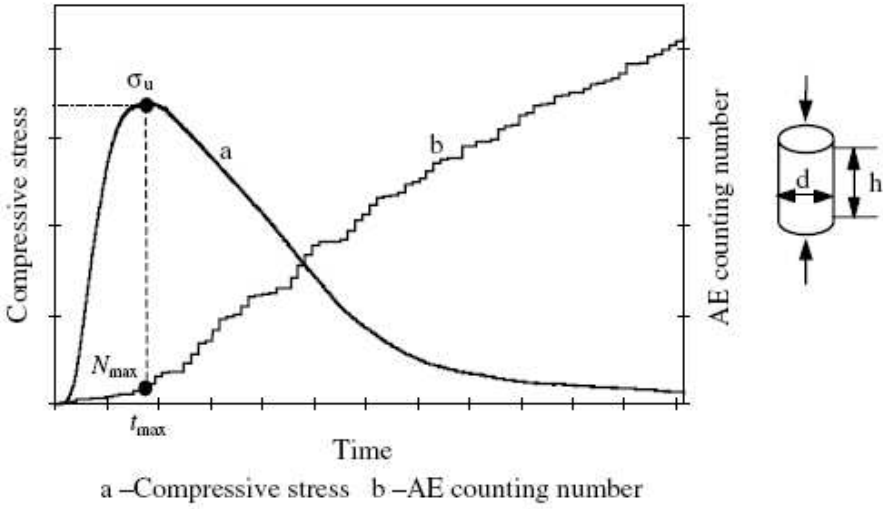


Figure 2: Stress and cumulated event number versus time.

Table 1: Experimental values obtained on concrete samples from pilaster P1.

| Specimen Type | Diameter *d* [mm] | Slenderness $\lambda=h/d$ | Experimental peak stress [Mpa] | $N_{max}$ at $\sigma_u$ | Numerical peak stress [Mpa] |
|---|---|---|---|---|---|
| C11 | 27.7 | 0.5 | 91.9 | 1186 | 46.9 |
| C12 | 27.7 | 1.0 | 62.8 | 1191 | 48.0 |
| C13 | 27.7 | 2.0 | 48.1 | 1188 | 46.2 |
| C21 | 59.0 | 0.5 | 68.1 | 8936 | 45.8 |
| C22 | 59.0 | 1.0 | 53.1 | 8934 | 47.8 |
| C23 | 59.0 | 2.0 | 47.8 | 8903 | 47.5 |
| C31 | 94.0 | 0.5 | 61.3 | 28502 | 46.4 |
| C32 | 94.0 | 1.0 | 47.8 | 28721 | 46.1 |
| C33 | 94.0 | 2.0 | 44.1 | 28965 | 45.9 |

The stress and cumulated event number versus time for a specimen of intermediate size is represented in Fig. 5b. In the figure the critical number of AE cumulative events $N_{max}$ is represented in correspondence of the peak stress $\sigma_u$. Similar results can be observed in the other cases.

2.2 *Numerical results*

The numerical models of the pure compression tests were built accounting for the presence of aggregates and of the cementitious matrix. Quadratic elements were used to represent both the aggregates and the matrix, while special interface elements were placed in between the two phases. The adopted mesoscale modeling directly accounts for the aggregate dimensional distribution, being each aggregate explicitly represented. The failure of the two phases was assumed as driven by plasticity in compression, with parabolic relation, and by linear softening in tension. A rotating smeared crack model based on total deformation was used. In order to avoid mesh dependency, the constitutive law for continuum elements is regularized providing that the area beneath the stress strain diagram in tension is equal to the tensile fracture energy divided by the crack bandwidth (i.e. the element size). The constitutive relation for interfaces was assumed elastic in compression and linear softening in tension. Since the constitutive law for interface elements is directly formulated in terms of stress vs. crack opening displacement (i.e. a cohesive law is assigned), no further regularization is necessary. All the analyses were performed with the Finite Element Software DIANA 9.2 [12]. The distribution of aggregate size and position was generated with the help of the module LATTICE of the program, according to the Füller distribution. The mechanical properties of the materials are summarized in Table 2. Figure 6 shows the mesh used to model the C2(1-3) specimens.

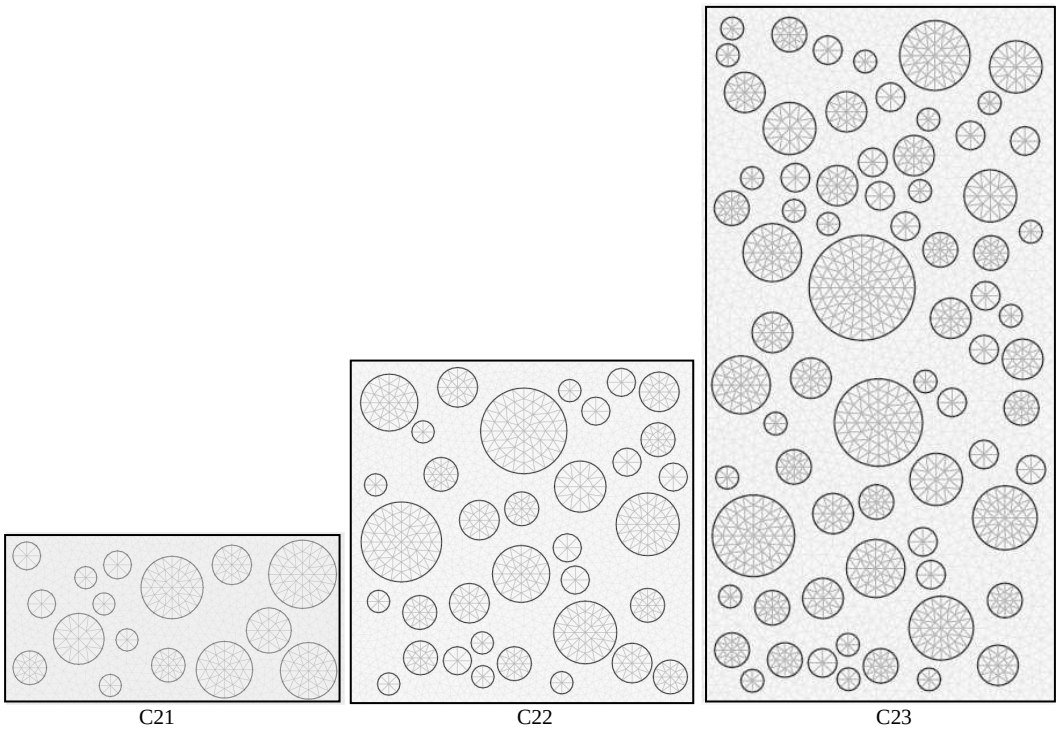


Figure 3: Three meshes of the modelled specimens.

Table 2. Mechanical properties adopted in the analysis.

| | | Aggregate | Matrix | Interface |
|---|---|---|---|---|
| Young's modulus | $E$ | $7.0\ 10^9$ Pa | $2.5\ 10^9$ Pa | $10.0\ 10^9$ N/m |
| Poisson ratio | $\nu$ | 0.15 | 0.15 | ---- |
| Tensile strength | $f_t$ | $10.0\ 10^6$ Pa | $5.0\ 10^5$ Pa | $2.0\ 10^5$ Pa |
| Fracture energy | $G_f$ | 60 N/m | 6 N/m | 3 N/m |
| Compressive strength | $f_c$ | ----- | $5\ 10^7$ Pa | ---- |

Figure 4a shows the boundary conditions and the load scheme of one of the specimens. Perfect friction between the loading platens and the specimen was assumed. In order to control the loading scheme with the arc-length algorithm, only the horizontal displacements of the top of the specimen were fixed, while the vertical displacements were kept equal by means of additional tying constrains. Figure 4b shows the typical barrel-shaped deformed mesh that is obtained under the above assumptions.

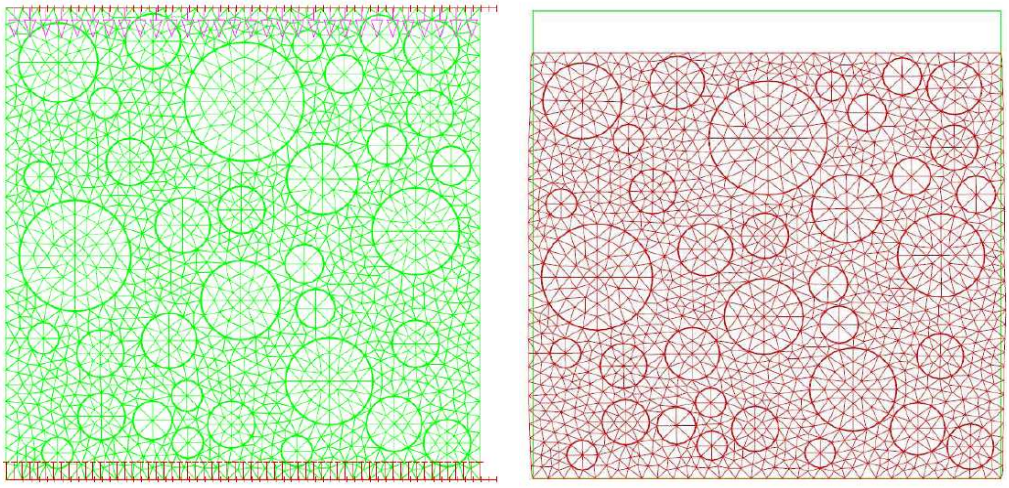

(a) (b)

Figure 4: Loading scheme and boundary condition of the specimen C22 (a); deformed shape (b).

Figure 5 shows the load-displacement curve obtained for the specimen C22. In general, accounting for cracking only it is not sufficient to correctly simulate the peak load, and the crushing of the matrix has necessarily to be taken into consideration. For this reason, the compressive behavior of the matrix is assumed as elastic perfectly plastic. On the other hand, the simulation of the post peak branch of the load displacement curve is cumbersome, and many convergence issues arise. Fortunately, the post peak regime was not of prior interest for the following analyses.

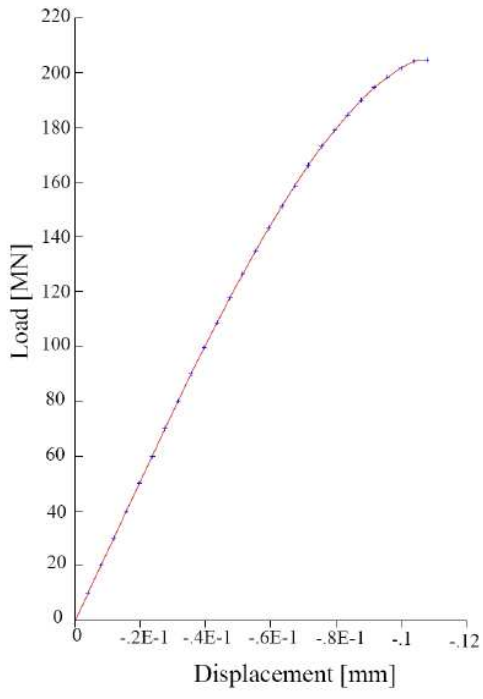


Figure 5: Load-displacement .

Figure 6 shows the localization of the matrix crushing in correspondence of the zones comprised among the most loaded aggregates. The crushed zones reveal sub-vertical patterns, similarly to what is observed for cracking.

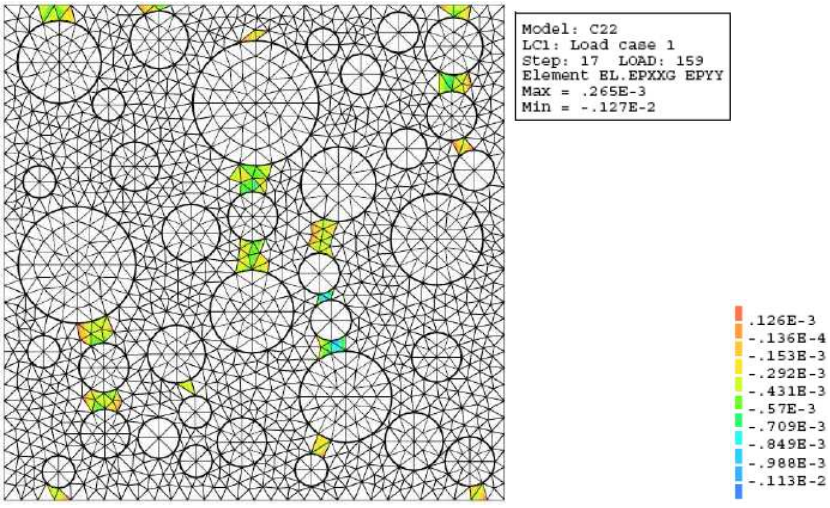


Figure 6: Crushing in the matrix of the specimen C22.

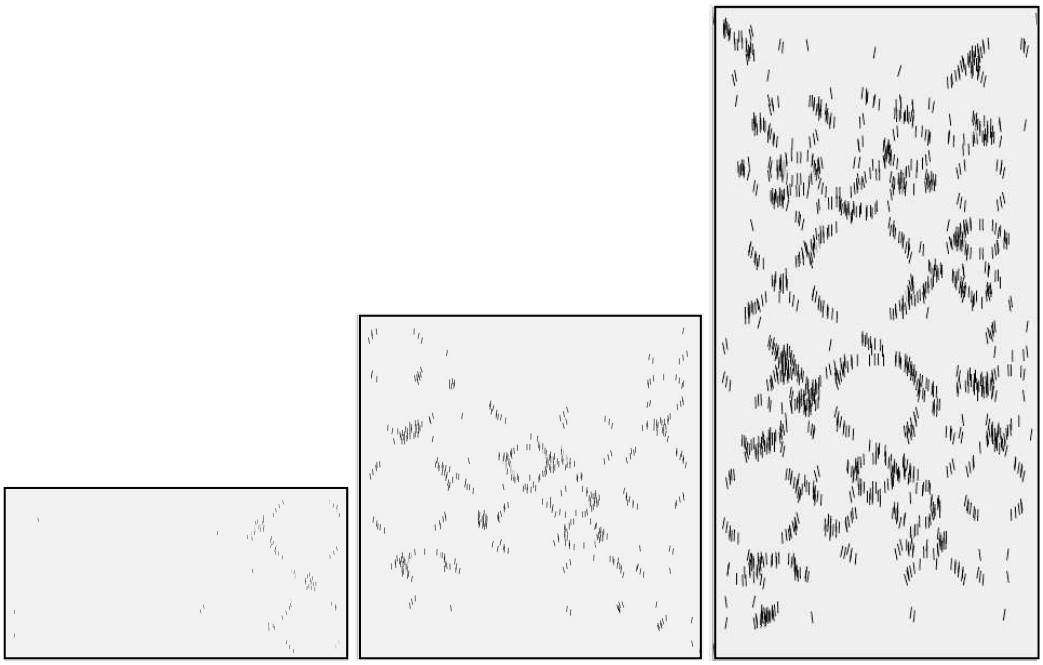

Figure 7: Crack patterns in specimens C12, C22 and C23.

The crack pattern for the three C2(1-3) samples is shown in Figure 7. It slightly changes varying the size, according to the different aspect ratios.

## 3 COMPARISON BETWEEN FRACTURE AND AE SCALING

In previous works [4-6], a statistical and fractal analysis of data from laboratory experiments was performed, considering the multiscale aspect of cracking phenomena. The fractal criterion takes into account the multiscale character of energy dissipation and the strong size effects associated with it. This makes it possible to introduce a useful energy-related parameter for the damage determination of full-size structure, by comparing the AE monitoring results with the values obtained on a reference specimen sampled from the structure and tested up to failure. This approach has been exploited by the Authors also for the interpretation of double flat-jack tests performed in historical masonry walls [10,11,13].

Fragmentation theories have shown that, during microcrack propagation, energy dissipation occurs in a fractal domain comprised between a surface and the specimen volume $V$ [8,9]. This implies that a fractal energy density (having anomalous physical dimensions):

$$\Gamma = \frac{W_{\max}}{V^{D/3}}, \tag{1}$$

can be considered as the size-independent parameter. In the fractal criterion of Eq. (1), $W_{\max}$ = total

dissipated energy; $\Gamma$= fractal energy density; and $D$ = fractal exponent comprised between 2 and 3.

On the other hand, during microcrack propagation, acoustic emission events can be clearly detected. Since the energy dissipated, $W$, is proportional to the number of the oscillations counts $N$, related to the AE events, $\Gamma_{AE}$ can be considered as a size-independent parameter:

$$\Gamma_{AE} = \frac{N_{\max}}{V^{D/3}}, \tag{2}$$

where $\Gamma_{AE}$ = fractal acoustic emission event density; and $N_{\max}$ is evaluated at the peak stress, $\sigma_u$. Eq. (2) predicts a volume effect on the maximum number of AE events for a specimen tested up to the peak stress.

The extent of structural damage in a full-size structure can be worked out from the AE data recorded on a reference specimen (subscript $r$) obtained from the structure. From Eq. (2) we get:

$$N_{\max} = N_{\max,r}\left(\frac{V}{V_r}\right)^{D/3}, \tag{3}$$

from which we can obtain the structure critical number of AE events $N_{\max}$.

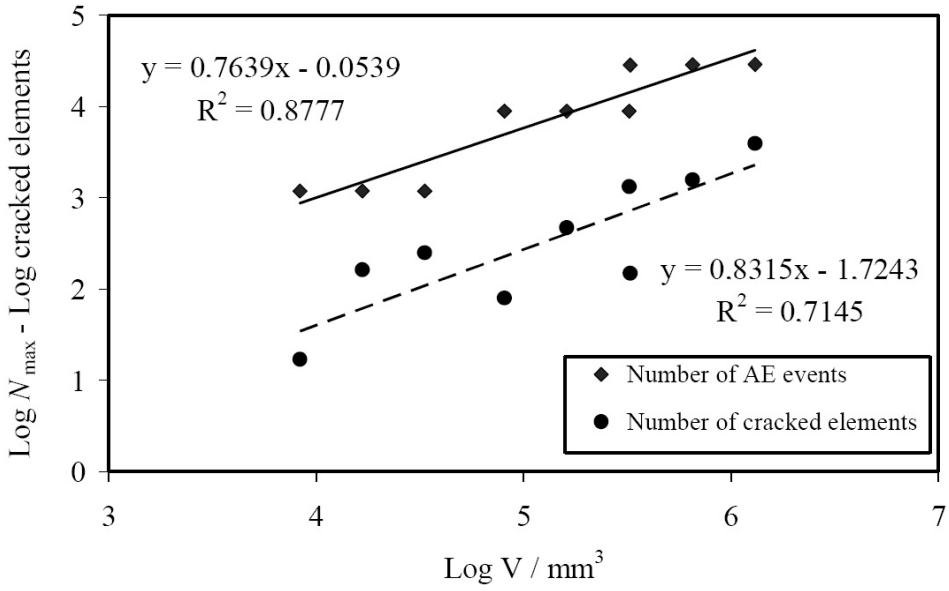


Figure 8: Scale effect on $N_{\max}$ and on the number of cracked finite elements.

Now, we can verify that the AE counting number is also proportional to the number of Gauss points subjected to cracking in the finite element model. Therefore, the number of AE and the number of cracks in the finite element model should show the same exponent with respect to the considered volume. In fact, this is what we can substantially observe from Figure 8 considering the

nine different specimens. For these reasons, it is possible to say that the numerical model is able to describe correctly the decrease in crack density with increasing specimen size.

Finally, let us observe that the intercept of this relation depends on the discretization of the finite element model. On the other hand, refining the mesh does not change sensibly the exponents reported in Figure 8.

## 4 CONCLUSIONS

A numerical simulation of an innovative concrete compression test combined with acoustic emission monitoring has been proposed. The numerical results agree rather well with the experimental evidences, and the crack patterns are simulated correctly. On the other hand, the model is not able to describe the decrease of the overall strength with increasing size, probably due to the introduction of the limit compression strength to model the crushing of the matrix, or to more fundamental reasons.

In addition, the number of acoustic emissions is put into relation with the number of Gauss points in the finite element model where cracking takes place. A good correlation is found between the amount of cracking simulated numerically and the experimental acoustic emission counting for different specimen sizes.

Although it is impossible to easily obtain a direct relation between the acoustic emission and the amount of cracking, nevertheless it is possible to state that the two quantities are proportional to each other when increasing sizes are considered.

*References*


[1] A. Carpinteri, P. Bocca, *Damage and Diagnosis of Materials and Structures*, Pitagora Editrice, Bologna, Italy. (1991).

[2] A. Anzani, L. Binda, G. Mirabella Roberti, "The effect of heavy persistent actions into the behavior of ancient masonry". *Materials & Structures*, **33**, 251-261 (2000).

[3] A. Carpinteri, G. Lacidogna, N. Pugno, "Structural damage diagnosis and life-time assessment by acoustic emission monitoring", *Engineering Fractures Mechanics*, **74**, 273-289 (2007).

[4] A. Carpinteri, S. Invernizzi, G. Lacidogna, "Structural assessment of a XVIIth century masonry vault with AE and numerical techniques", *International Journal of Architectural Heritage*, **1**(2), 214-226 (2007).

[5] A. Carpinteri, G. Lacidogna, "*Structural monitoring and integrity assessment of medieval towers*", *Journal of Structural Engineering (ASCE)*, **132**, 1681-1690 (2006).

[6] A. Carpinteri, G. Lacidogna, "Damage monitoring of a masonry building by the acoustic emission technique". *Materials & Structures*, **39**, 161-167 (2006).

[7] A. Carpinteri, N. Pugno, "Fractal fragmentation theory for shape effects of quasi-brittle materials in compression". *Magazines Concrete Research*, **54**(6), 473-480, (2002).

[8] A. Carpinteri, N. Pugno, "A fractal comminution approach to evaluate the drilling energy dissipation". *International Journal for Numerical and Analytical Methods In Geomechanics*, **26**(5) 499-513, (2002).

[9] A. Carpinteri, N. Pugno, "A multifractal comminution approach for drilling scaling laws". *Powder Technology*, **131**(1), 93-98, (2003).

[10] ASTM, "Standard test method for in situ measurement of masonry deformability properties the using flat-jack method", *ASTM C1197-91*, Philadelphia, (1991).

[11] G. Sacchi Landriani, A. Taliercio, "Numerical analysis of the flat jack test on masonry walls", Journal of Theoretical and Applied Mechanics, **5**(3), 313-339, (1986).

[12] F.C. de Witte, G.J. Schreppers, *DIANA Finite Element Analysis User's Manual*, TNO DIANA BV, Delft, The Netherlands, (2007).
[13] A. Carpinteri, S. Invernizzi, G. Lacidogna, "Historical brick-masonry subjected to double flat-jack test: Acoustic Emissions and scale effects on cracking density", *Construction and Building Materials*, **23**(8), 2813-2820, (2009).